Phytosphingosine and Sphingosine Ceramide Headgroup Hydrogen Bonding: Structural Insights through Thermotropic Hydrogen/Deuterium Exchange

ARTICLE *in* THE JOURNAL OF PHYSICAL CHEMISTRY B · AUGUST 2001

Impact Factor: 3.3 · DOI: 10.1021/jp0118367

6 AUTHORS, INCLUDING:

Mark Rerek
Chemtrade Logistics
32 PUBLICATIONS **1,318** CITATIONS
SEE PROFILE

Patrick Garidel
Martin Luther University Halle-Wittenberg
148 PUBLICATIONS **3,157** CITATIONS
SEE PROFILE

Richard Mendelsohn
Rutgers, The State University of New Jersey
168 PUBLICATIONS **4,824** CITATIONS
SEE PROFILE

David J Moore
GlaxoSmithKline plc.
85 PUBLICATIONS **1,888** CITATIONS
SEE PROFILE

Phytosphingosine and Sphingosine Ceramide Headgroup Hydrogen Bonding: Structural Insights through Thermotropic Hydrogen/Deuterium Exchange

Mark E. Rerek,*,† Hui-chen Chen,‡ Berislav Markovic,† Dina Van Wyck,† Patrick Garidel,‡ Richard Mendelsohn,‡ and David J. Moore§

International Specialty Products, Wayne, New Jersey 07040, Department of Chemistry, Rutgers University, Newark, New Jersey 07102, and Unilever Research US, Edgewater, New Jersey 07020

Received: May 14, 2001

IR spectroscopic studies are reported for the phytosphingosine class of ceramides and are compared with two analogous sphingosine ceramides. The phytosphingosine class of molecules, not previously widely investigated by physical techniques, constitutes ∼30% of the total ceramide content of the stratum corneum, the barrier to permeability in skin. The current measurements utilize temperature-controlled horizontal attenuated total reflectance spectroscopy of hydrated films to study H → D exchange in the polar regions of the molecules as well as chain conformational order and packing properties. Analysis of the methylene stretching and scissoring vibrations reveals that the chains of the two phytosphingosine derivatives (ceramides 3 and 7) are much more poorly packed at room temperature than their sphingosine counterparts (ceramides 2 and 5 respectively), despite having order → disorder transitions some 15−20 degrees higher. This unanticipated relative stability of the phytosphingosines is traced to enhanced headgroup H-bonding interactions manifest by lower Amide I and higher Amide II frequencies. Water penetration into the polar regions is monitored by the temperature dependence of the Amide II and O−H/N−H stretching intensities as a function of H→D exchange. Neither ceramide 2 nor 3 exchanges N−H or O−H protons until relatively high temperatures (>65 °C). However, addition of an α-hydroxy group on the fatty acid chain in ceramides 5 or 7 results in exchange events observed at temperatures much closer to physiological. These measurements reveal that the relative contributions of chain packing and H-bonding under physiological conditions differ markedly for the phytosphingosines compared to the sphingosines. The former are characterized by hexagonal chain packing with relatively strong H-bonding; the latter by orthorhombic chain packing and weaker H-bonding. The implications of these molecular structure data for lipid organization in the stratum corneum are briefly discussed.

1. Introduction

The barrier function of skin resides in the lipid component of the stratum corneum. This outer layer of the epidermis is composed of terminally differentiated, keratin-filled, elongated, and flattened corneocytes, surrounded by an extracellular lamellar lipid matrix.[1] The lipid composition is unusual, consisting of a roughly equimolar mixture of ceramides, free fatty acids, and cholesterol, along with cholesterol esters and cholesterol sulfate.[2−4] To understand the complex lipid architecture underlying skin barrier function, our laboratories are investigating the fundamental molecular biophysics of hydrated stratum corneum lipids.[5−9] Such studies are needed because ceramides exhibit quite different molecular phase behavior than phospholipids and other more widely studied biological membrane lipids. The plethora of recent reports on the biological importance of ceramides in cell signaling further underscores the importance of understanding their molecular behavior.[10−12]

At least eight distinct ceramide species have been identified in human stratum corneum, all with fatty acid chains generally longer than C-20.[13−15] These ceramides fall into two main classes, sphingosines and phytosphingosines, names which describe the nature of their base chains. We will use the numbering nomenclature of Downing and co-workers following their discovery of the latest ceramide species, which are a subclass of the sphingosines based on 6-hydroxysphingosine.[15] The main consequences of their findings are to add ceramide 6 and ceramide 8, moving the previously designated phytosphingosine ceramide 6 to ceramide 7 according to the TLC position of the materials. They showed that the new ceramide 6 was in intimate mixture with ceramide 5; only after acetylation could these materials be resolved from each other, thus adding an additional ceramide between 5 and the formerly designated ceramide 6.

The majority of biophysical reports published to date on one component ceramide systems have focused on sphingosine ceramides. The most general finding of this work has been that ceramides are extremely ordered and minimally hydrated molecules at physiological temperatures. Our FTIR spectroscopy studies have demonstrated that sphingosines pack in orthorhombic phases with strong intermolecular hydrogen bonding between the headgroups of adjacent molecules.[6,16,17]

The current investigation probes three ceramide molecules from the phytosphingosine class of ceramides. The phytosphingosine ceramides do not possess a 4,5 trans double bond but have an additional hydroxyl group on the base chain 4 position and thus can be thought of as hydrated sphingosines,

* To whom correspondence should be addressed. Mark Rerek, International Specialty Products, 1361 Alps Road, Wayne, NJ 07040. Tel: 973-872-4307. Fax: 973-628-3401. E-mail: mrerek@ispcorp.com.

† International Specialty Products.

‡ Rutgers University, Department of Chemistry.

§ Unilever Research US.

10.1021/jp0118367 CCC: $20.00
Published on Web 08/25/2001

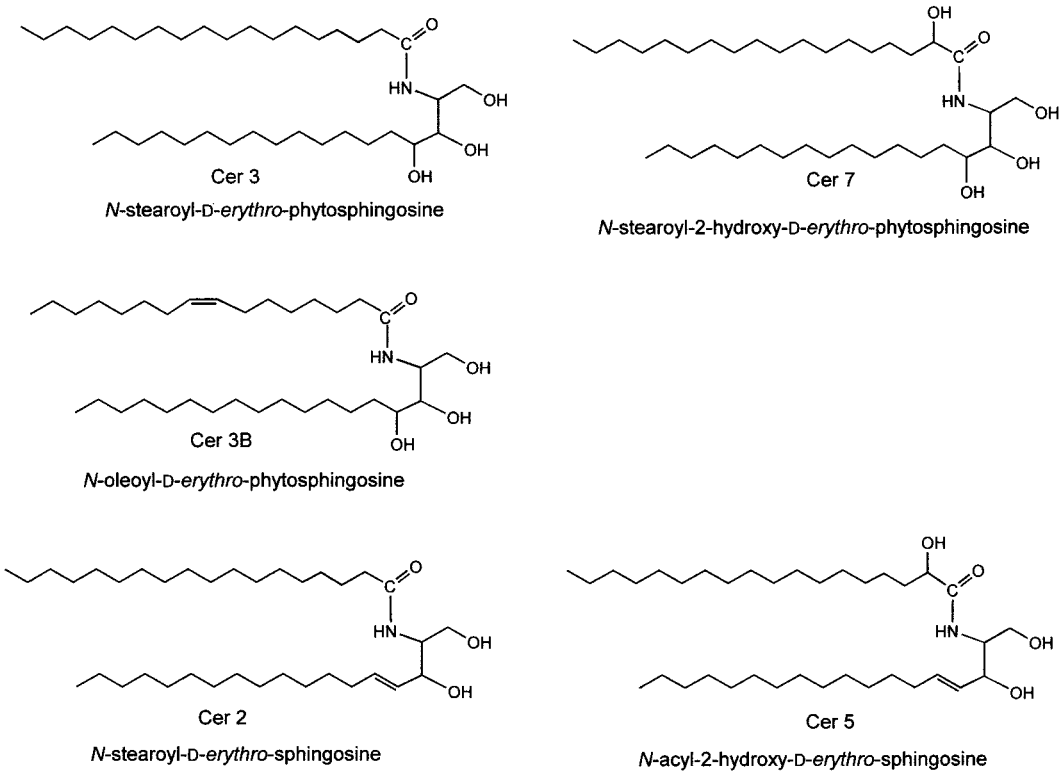

Figure 1. Chemical structures of the ceramides used in this study and their abbreviations.

or conversely, sphingosines can be thought of as dehydrated phytosphingosines. It should be noted, however, that the enzymatic pathways by which all the various ceramides species are synthesized in skin are not yet clearly determined.[18]

Phytosphingosines account for about 25 to 35% of total stratum corneum ceramide content, with ceramide 3 being approximately twice as abundant as ceramide 7 (one of the least common ceramides). Ceramide 3 is the phytosphingosine equivalent of ceramide 2 and ceramide 7 is the phytosphingosine equivalent of ceramide 5. Ceramides 5 and 7 both possess an α-hydroxy group on the fatty acid chain. Among the few published biophysical studies of these lipids the most notable are the monolayer studies of Pascher and co-workers, which report that phytosphingosines have a much larger molecular area than their sphingosine analogues.[19] The phytosphingosine ceramide molecules and their sphingosine equivalents are shown in Figure 1.

The current work reports our findings from studies of phytosphingosine ceramides corresponding to human stratum corneum ceramides 3 and 7. Specifically, these studies use analogues of ceramide 3 (Cer 3) and 7 (Cer 7) with pure C18 base and stearyl fatty acid chains, and a synthetic analogue of ceramide 3 (Cer 3B) with an oleoyl fatty acid chain. This modification reduces the melting temperature of Cer 3B below 100 °C thereby permitting straightforward manipulation of the molecule in aqueous systems.

The present study utilizes Fourier transform infrared (FTIR) spectroscopy to study ceramide films under both H_2O and ^2H_2O buffers as a function of temperature. This approach allows detailed analysis of both the chain and headgroup behavior of the phytosphingosine ceramides. Although we have previously reported some information on amide N−H → N−D exchange in two fatty acid heterogeneous sphingosine ceramides, Cer 2 and Cer 5, we have not reported on hydroxyl exchange (O−H → O−D) or the temperature dependence of the exchange processes.[6,17] Therefore, we present the dynamics of the deuterium exchange of a synthetic analogue of ceramide 2 (Cer 2) containing stearyl fatty acid chains and a bovine brain derived natural equivalent to ceramide 5 (Cer 5). This provides a coherent view of hydrogen bonding effects in the major ceramide components of the stratum corneum. It is interesting to note that previous authors have raised the issue of hydrogen bonding and speculated upon its potentially critical role as a cohesive force in lipid membranes.[20,21]

The current study on phytosphingosine derivatives provides a detailed picture of the molecular organization and phase behavior under highly controlled conditions. Given the critical role that ceramides play in stratum corneum barrier function, this picture adds to our understanding of the contributions that phytosphingosines in particular, and headgroup hydrogen bonding in general, make to the cohesion, integrity, and function of the lipid skin barrier.

2. Experimental Section

Materials. Synthetic nonhydroxylated sphingosine ceramide (N-stearyl-D-*erythro*-sphingosine), equivalent to human ceramide 2 (Cer 2) was purchased from Northern Lipids (Vancouver, Canada). Bovine brain hydroxy fatty acid ceramide, (N-acyl-2-hydroxy-D-*erythro*-sphingosine), equivalent to human ceramide 5 (Cer 5), was purchased from Sigma Chemical Co. (St. Louis, MO.) The fatty acid chain length distribution is primarily C18:0, C22:0, C24:0, and C24:1. Ceramide III (N-stearyl-D-*erythro*-phytosphingosine), equivalent to human ceramide 3 (Cer 3), Ceramide IIIB (N-oleoyl-D-*erythro*-phytosphingosine), not a physiological ceramide but referred to as ceramide 3B (Cer 3B) in this study, and ceramide VI (N-stearyl-2-hydroxy-D-*erythro*-phytosphingosine), equivalent to human ceramide 7 (Cer 7) were obtained from Cosmoferm, CT. The structures of the ceramides and their abbreviations are shown in Figure 1.

FTIR Spectroscopy. Ceramide samples for FTIR spectroscopy measurements were prepared by adding 6 mg of each

ceramide, dissolved in 150 μL of $CHCl_3/CH_3OH$ (2:1), to a ZnSe crystal mounted in a trough plate and placed in a temperature-controlled, horizontal attenuated total reflectance (HATR) setup (Spectra-Tech, Shelton, CT). After evaporation of the organic solvent, lipid films were further dried under high vacuum for at least 1 h. The dried lipid films were first hydrated with H_2O by slowly heating to 90 °C, and cooling to 25 °C. During the cooling cycle, H_2O was allowed to evaporate. To the maximally hydrated ceramide samples, 2 mL of D_2O were added, and a cover plate was placed over the trough to prevent D_2O evaporation before data collection. Some ceramide samples were left at room temperature for 24 h before adding D_2O and beginning data acquisition. For some of the Cer 3 experiments, the hydrated lipid samples were held at 90 °C, and spectra collected every 5 min for 1 h. All experiments were repeated several times and gave equivalent results in all cases.

Fourier transform infrared (FTIR) spectra were collected on a Mattson RS1 spectrometer equipped with a broad band mercury−cadmium-telluride (MCT) detector and kept under continuous dry air purge. Spectra were generated by co-addition of 256 interferograms collected at 2 cm^{-1} resolution, apodized with a triangular function and Fourier transformed with one level of zero filling. Spectra were routinely acquired at 2 °C intervals from 25 up to 98 °C. Data were analyzed off-line with software written at the National Research Council of Canada and plotted with Sigma Plot 5.0 (SPSS, IL).

Differential Scanning Calorimetry (DSC). Hydrated ceramide samples were prepared by adding 40 μL of H_2O to stainless steel DSC pans (LVC, Perkin−Elmer) containing weighed samples (2−3 mg) of ceramides, and then sealed. All samples were kept at −10 °C before measurements. Calorimetric measurements were performed with a Perkin−Elmer Pyris-1 DSC differential scanning calorimeter (Norwalk, CT) at a heating rate of 1 and 5 °C per min. To ensure sample hydration and measurement reproducibility, three consecutive heating and cooling scans of each sample from 25 to 100 °C at 5 °C/min were conducted before the final thermograms were recorded from 25 to 125 °C at a scan rate of 1 °C/min. Duplicate runs of the same sample gave onset, midpoint, and completion temperatures reproducible to 1 °C. Data were analyzed using the Perkin-Elmer Thermal Data Analysis software.

Structure Calculations. HyperChem (Hypercube) was used to generate the molecular structure of tetracosanoylphytosphingosine using the structural parameters given in Pascher's paper.[22]

3. Results

Table 1 summarizes the key results for each ceramide. Included are the frequencies of the CH_2 symmetric stretching mode ($\nu_{sym}CH_2$), the CH_2 scissoring mode (δCH_2), the OH/NH stretching modes (νOH/νNH), Amide I and II frequencies, and the temperature of the chain disordering transition. Each of the phytosphingosines, designated Cer 3, Cer 7, and Cer 3B, have an initial $\nu_{sym}CH_2$ between 2848.6 and 2849.6 cm^{-1}, characteristic of all-trans, conformationally ordered chains (even for the oleoyl containing Cer 3B). The lower $\nu_{sym}CH_2$ values of the sphingosines Cer 2 and Cer 5, 2847.7, and 2846.2 cm^{-1} respectively, are consistent with tightly packed conformationally ordered chains. Consistent with their methylene symmetric stretching frequencies, each of the phytosphingosines has a single δCH_2 peak at 1467 cm^{-1} indicating hexagonal chain packing. In contrast to the phytosphingosines, the sphingosines (Cer 2 and 5) exhibit splitting of the δCH_2 mode into two peaks, which is characteristic of chains packed in a perpendicular orthorhombic subcell phase.

TABLE 1: Infrared Parameters that Provide Structural Information for Ceramides[a]

ceramide	νOH/νNH	amide I	amide II	δCH_2	$\nu_{sym}CH_2$	*Tm*, °C
cer 3	3368	1612	1556	1467	2848.6	115
	3329					
cer 3B	3374	1612	1556	1467	2849.6	87
	3326					
cer 7	3322	1620	1545	1467	2849.0	93
cer 2	3359	1644	1550	1470	2847.7	93
	3310	1619		1464		
cer 5	3443	1645	1523	1469	2846.2	78
orthorhombic	3353	1630	1519	1462		
	3266					
cer 5	3322	1638	1536	1467	2850.0	78
hexagonal		1632	1532			

[a] IR peaks are in cm^{-1} and are measured from spectra acquired at 27 °C. Tm values are either from DSC or from the midpoint of the temperature-induced change in the CH_2 symmetric stretching vibration.

As detailed in Table 1 the phytosphingosines exhibit lower Amide I frequencies and higher Amide II frequencies (both behaviors indicative of stronger hydrogen bonding) than the corresponding sphingosines.

With the exception of Cer 7 and hexagonally packed Cer 5, all the ceramides studied here have well resolved peaks in the 3200−3500 cm^{-1} region. These peaks arise from O−H and/or N−H stretching modes (νOH or νNH). Without isotopic labeling, it is impossible to make definitive assignments for the observed peaks. In the presence of ^2H_2O, all of the ceramides studied here undergo H → D exchange of both their amide and hydroxyl groups, to a greater or lesser extent, depending on temperature. These processes can be directly monitored via the decrease in integrated areas of the Amide II and hydroxyl/amide stretching (νOH/νNH) contours. Figures 2 and 3 show representative spectra of the νOH/νNH (3000−3700 cm^{-1}) and the Amide I and II (1500−1700 cm^{-1}) spectral regions, respectively, of Cer 3, Cer 3B, and Cer 7 in the presence of ^2H_2O and collected at ∼2° intervals from 25 to 98 °C. The decrease in integrated areas of the Amide II and νOH/νNH modes were measured as a function of temperature, normalized to the area of the methylene stretches, and adjusted to a relative 0−1 scale, to enable direct comparison of changes in areas.

The thermotropic behavior of Cer 3 is shown in Figure 4. The relatively small increase in the symmetric methylene stretching frequency from 2848.5 to 2849.2 cm^{-1} indicates no major change in chain conformation by 100 °C (the practical limit of these HATR experiments). DSC measurements revealed that chain melting occurs at 115 °C. At 75 °C the hydroxyl O−H and amide N−H begin H → D exchange in a synchronous manner, as revealed by the plots of νOH/νNH and Amide II areas in Figure 4. Most of the amide and hydroxyls are exchanged before 100 °C.

Both the initial spectra and the OH/NH exchange behavior of Cer 3 and Cer 3B are very similar (Figures 2 and 3). Figure 5 shows the thermotropic exchange behavior of Cer 3B, which begins around 65 °C and proceeds to completion just prior to the chain disorder transition at 87 °C. From the spectra in Figure 2, it seems the 3380 cm^{-1} peak is lost before the 3330 cm^{-1} peak although quantitative analysis is rendered difficult by the nonlinear baselines and changing peak widths. In concert with H → D exchange, Amide I shifts from 1612 to 1606 cm^{-1} before broadening and increases to 1628 cm^{-1} after chain conformational disordering. As shown in Figure 5, the normalized change in the OH/NH stretching contour and Amide II areas with increasing temperature are similar. This indicates that the hydroxyl and amide H → D exchange occur essentially in parallel.

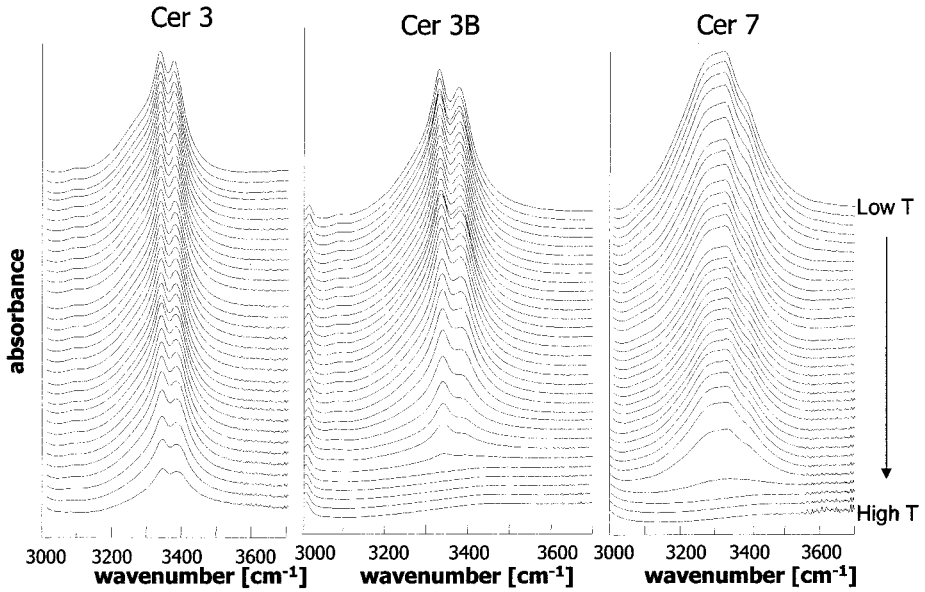

Figure 2. Changes in νOH/νNH spectral region as a function of temperature and H → D exchange for Cer 3, Cer 3B, and Cer7.

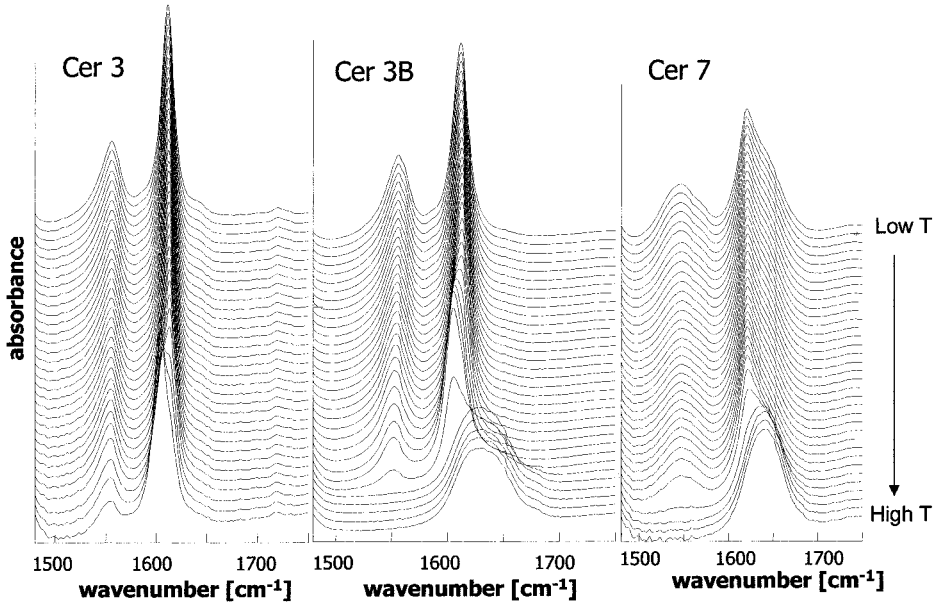

Figure 3. Changes in Amide I and Amide II spectral region as a function of temperature and H → D exchange for Cer 3, Cer 3B, and Cer 7.

As shown in Figure 6, the onset of OH and NH exchange begins at 25 °C for Cer 7 (see spectra in Figures 2 and 3). Exchange occurs more rapidly for the νOH/νNH contour than for the Amide II mode up to 50 °C. At that point, the νOH/νNH contour has lost 35−40% of its initial area while the Amide II area has only diminished by ∼15%. The OH bonds are thus more extensively exchanged than the NH at this point. (If both the OH and NH had each exchanged to the same extent, then the νOH/νNH contour would have lost ∼15% of its initial area.) From 60 to 80 °C, the exchange monitored by νOH/νNH contour slows but never stops, whereas the Amide II exchange is essentially completely halted. This again suggests that for Cer 7, the accessibility of at least some of the O−H bonds to solvent is greater than for the amide hydrogen. Above ∼90 °C, both the Amide II and νOH/NH complete H → D exchange in concert with chain disordering. Amide I shifts from 1620 to 1640 cm^{-1} after H → D exchange and chain conformational disordering.

The thermotropic behavior of H → D exchange in Cer 2 is shown in Figure 7. Initially, two νOH/νNH peaks are observed at 3359 and 3310 cm^{-1} and, as we have previously reported for Cer 2, the Amide I mode is split into two components. As shown in Figure 7, the νOH/νNH exchange is reasonably synchronous with amide NH exchange. Thus, as for Cer 3, the labile protons are equally accessible to H → D exchange. As we previously reported, some H → D exchange occurs at the orthorhombic → hexagonal phase transition temperature (65−70 °C). However, complete exchange in Cer 2 does not occur until chain disordering.

Figure 8 shows the synchronous H−D exchange of νOH/νNH and Amide II for orthorhombically packed Cer 5. Exchange begins at 25 °C and continues in a near linear manner with temperature until ∼5 °C before conformational disordering, when the process accelerates to completion. The normalized, temperature-dependent change in area for the νOH/νNH stretching contour and the Amide II modes are very similar.

It usually takes 12−24 h at room temperature for Cer 5 to re-order into an orthorhombic state after heating with buffer. Thus, it proved feasible to acquire IR spectra of the metastable

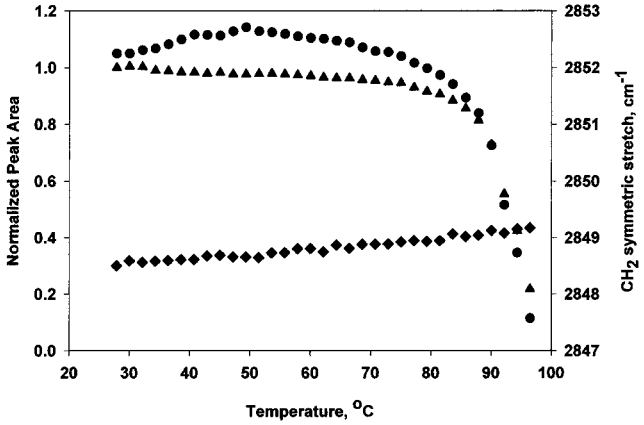

Figure 4. Thermotropic changes in $\nu_{sym}CH_2$ frequency, Amide II relative integrated area, and νOH/νNH relative integrated area during H → D for Cer 3. Legend: ◆ = $\nu_{sym}CH_2$ frequency, ● = νOH/νNH relative integrated area, ▲ = Amide II relative integrated area.

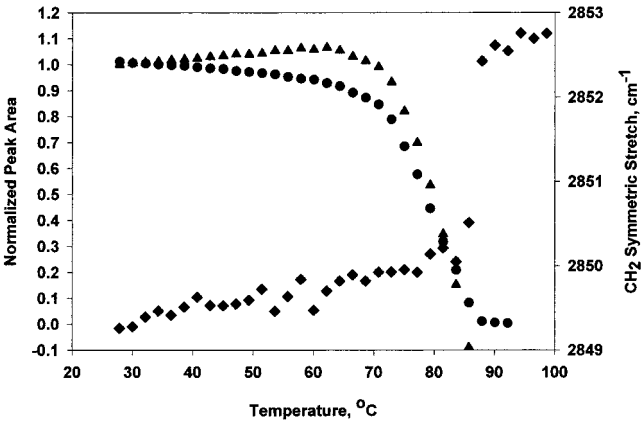

Figure 5. Thermotropic changes in $\nu_{sym}CH_2$ frequency, Amide II relative integrated area, and νOH/νNH relative integrated area during H → D for Cer 3B. Legend: ◆ = $\nu_{sym}CH_2$ frequency, ● = νOH/νNH relative integrated area, ▲ = Amide II relative integrated area.

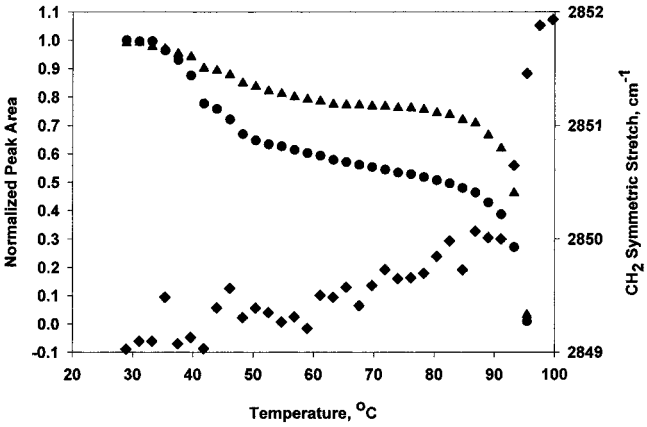

Figure 6. Thermotropic changes in $\nu_{sym}CH_2$ frequency, Amide II relative integrated area, and νOH/νNH relative integrated area during H → D for Cer 7. Legend: ◆ = $\nu_{sym}CH_2$ frequency, ● = νOH/νNH relative integrated area, ▲ = Amide II relative integrated area.

phase which is hexagonally packed, characterized by a $\nu_{sym}CH_2$ of 2849 cm^{-1}, and one broad νOH/νNH band centered at 3330 cm^{-1}. Despite the looser chain packing in this molecule, the H-bonds in the polar region are stronger as indicated mostly by increased Amide II frequencies (Table 1). Hexagonally packed Cer 5 undergoes rapid exchange of νOH/νNH and Amide II such that the process is complete by 45 °C. The two

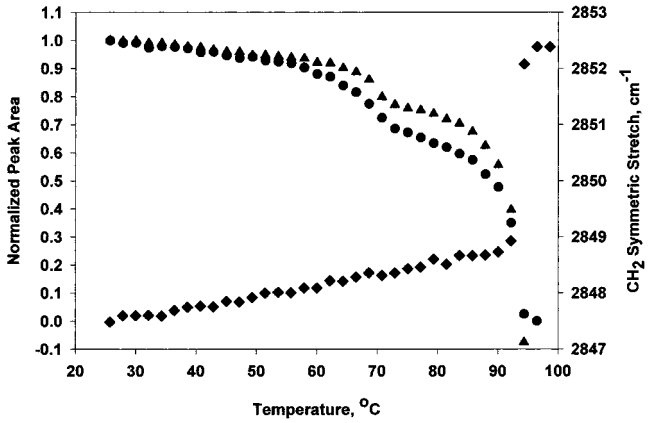

Figure 7. Thermotropic changes in $\nu_{sym}CH_2$ frequency, Amide II relative integrated area, and νOH/νNH relative integrated area during H → D for Cer 2. Legend: ◆ = $\nu_{sym}CH_2$ frequency, ● = νOH/νNH relative integrated area, ▲ = Amide II relative integrated area.

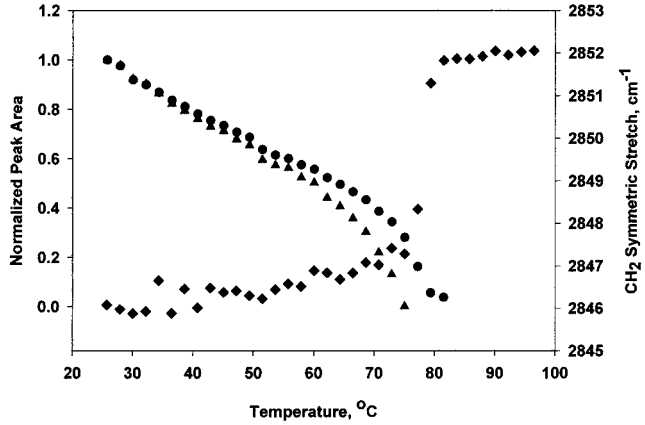

Figure 8. Thermotropic changes in $\nu_{sym}CH_2$ frequency, Amide II relative integrated area, and νOH/νNH relative integrated area during H → D for orthorhombic phase Cer 5. Legend: ◆ = $\nu_{sym}CH_2$ frequency, ● = νOH/νNH relative integrated area, ▲ = Amide II relative integrated area.

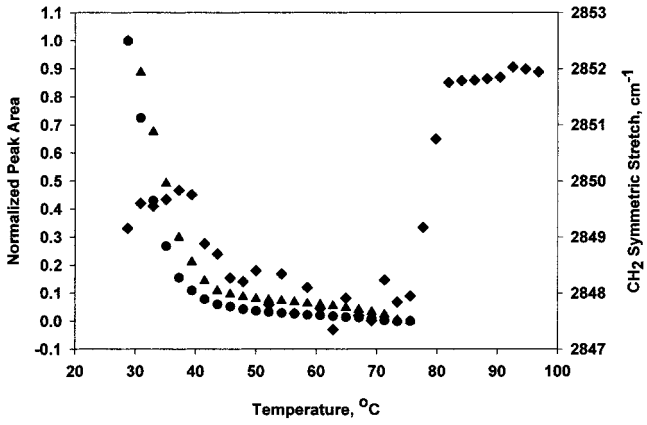

Figure 9. Thermotropic changes in $\nu_{sym}CH_2$ frequency, Amide II relative integrated area, and νOH/νNH relative integrated area during H → D for hexagonal phase Cer 5. Legend: ◆ = $\nu_{sym}CH_2$ frequency, ● = νOH/νNH relative integrated area, ▲ = Amide II relative integrated area.

spectral regions change in concert. These data are plotted in Figure 9.

4. Discussion

The power and utility of IR spectroscopy for elucidating molecular organization in ordered lipid phases in general, and

ceramide phases specifically, is clearly manifest in the current report. This work describes the impact upon molecular behavior that occurs with a single change in the chemical structure of a given ceramide, such as hydrating a double bond and/or adding a hydroxyl group next to the amide carbonyl. Such apparently small changes, which characterize different ceramide species, produce significant alterations in chain packing, chain conformational order, amide hydrogen bonding, hydroxyl hydrogen bonding, and the ability of water to penetrate the assembly of ceramide molecules. Each of these effects, which are conveniently monitored from IR spectral changes, will be considered in detail.

CH_2 Stretching Frequencies. The CH_2 stretching frequencies for each of the ceramides at 27 °C are shown in Table 1. It has been shown for many lipid systems that the appearance $\nu_{sym}CH_2$ below 2850 cm^{-1} is indicative of extended, ordered all-trans hydrocarbon chains. The actual frequency below 2850 cm^{-1} may monitor both chain geometry and packing.[23] The frequencies observed for the phytosphingosines studied indicate conformationally ordered chains at physiological temperatures, including somewhat unexpectedly, Cer 3B, which contains a cis double bond at the 9,10 position of the fatty acid chain.

Both of the physiological representative phytosphingosines, Cer 3 and Cer 7, have values of $\nu_{sym}CH_2$ approximately 2 cm^{-1} higher than their corresponding sphingosines (Cer 2 and Cer 5, respectively). This may be due to greater rotational freedom of the chains within the hexagonal geometric packing. Given the similarity in chain composition, this increase in packing freedom presumably results from the replacement of the trans double bond with a hydroxyl group. However, it is important to note that Cer 3 and Cer 7 disorder 22 and 15 °C *higher* than Cer 2 and Cer 5, respectively, despite more poorly packed chains. This rather unexpected result suggests that less tightly packed chains at room temperature do not necessarily indicate structures of reduced thermotropic stability. As discussed below, the additional thermal stability of the phytosphingosines must therefore be achieved through headgroup H-bonding interactions. Within the same ceramide class, the consequences upon chain phase behavior of the addition of an α-hydroxyl group are significant, producing a 22 °C decrease in transition temperature between the phytosphingosines, Cer 7 and Cer 3, and a 15 °C decrease between the sphingosines, Cer 2 and Cer 5. It should be noted that Cer 5 is the only ceramide in this study that has a mixture of chains; this could have an effect on the quantitative comparison of melting temperatures. All other ceramides possess C18 acid and base chains. However, it is clear that addition of an α-hydroxy group or going from phytosphingosine to sphingosine lowers the chain melting temperature. This further suggests that headgroup behavior such as H-bonding must play a significant role in the final determination of the order → disorder transition in the phytosphingosines.

CH_2 Scissoring Frequencies. Although $\nu_{sym}CH_2$ provides a measure for transition temperatures and chain conformational order, it does not unambiguously identify the nature of the phases present. We have previously reported a doublet in the δCH_2 mode of the sphingosines Cer 2 and Cer 5 that is characteristic of ordered orthorhombic subcells. However, the current work demonstrates Cer 5 can also form a metastable hexagonal phase upon cooling, which takes up to 72 h to fully rearrange to the orthorhombic phase. The phase has a characteristic single δCH_2 peak at 1467 cm^{-1}. Under the current experimental conditions, the phytosphingosine ceramides form phases with hexagonally packed chains, as revealed by the single δCH_2 peak at 1467 cm^{-1} at all stages of the heating or cooling cycle for Cer 3, Cer 3B, and Cer 7. As discussed above, the hexagonal packing of phytosphingosine chains is consistent with the higher $\nu_{sym}CH_2$ values compared with the analogous orthorhombically packed sphingosines. The sphingosines undergo a solid → solid-phase transition from orthorhombic to hexagonal packing characterized by a collapse of the scissoring doublet. The observed difference in the packing of phytosphingosines and sphingosines in bulk phases is consistent with the monolayer work of Lofgren and Pascher.[19] They reported the limiting area per molecule at zero surface pressure was 42 $Å^2$ and 44 $Å^2$ for Cer 2 and Cer 5, respectively, and 48 $Å^2$ for both Cer 3 and Cer 7. At surface pressures of 30 dyn/cm, the values were 40.5 $Å^2$ for Cer 2, 41.5 $Å^2$ for Cer 5, and 44 $Å^2$ for both Cer 3 and Cer 7. Recently, a value for Cer 3 from the same source as used here (Cosmoferm) was reported to be 43 $Å^2$ at 30 dyn/cm, in good agreement with the original measurement.[24] These findings are consistent with the conclusion from the current IR studies that phytosphingosines pack less tightly than sphingosines.

Amide Hydrogen Bonding. The strength of amide hydrogen bonding can be inferred from the frequencies of the Amide I and Amide II modes. As reported above, Cer 3 and Cer 3B have very low values of Amide I, about 1612 cm^{-1}, which is indicative of very strong H-bonding to the amide C═O, and is almost 20 cm^{-1} lower than the average frequency for Cer 2, the analogous sphingosine. A similar pattern is observed for α-hydroxy ceramides: Cer 7 has a lower value of Amide I (1620 cm^{-1}) compared to orthorhombic Cer 5 (average value of 1637 cm^{-1}). Equivalent and consistent trends are observed for Amide II behavior in all the above examples. The phytosphingosine and sphingosine ceramides with α-hydroxy fatty acid chains clearly have weaker amide hydrogen bonding than their analogous ceramides without the α-hydroxy group (as seen by the higher Amide I and lower Amide II frequencies). It is evident from these data that optimization of either chain packing or H-bonding determine the relative thermal stability of these phases. Interestingly, hexagonally packed metastable Cer 5 exhibits stronger amide hydrogen bonding than Cer 5 in the orthorhombic phase, as reflected by a decrease in Amide I by 3 cm^{-1} and an increase in Amide II by 13 cm^{-1}.

Hydroxyl and Amide Hydrogen Exchange. From the data reported in this study on H → D exchange of ceramide hydroxyl and amide groups, several inferences can be drawn concerning the importance of hydrogen bonding to the overall molecular organization of ceramides. The initial inability of ^2H_2O to penetrate the polar regions (i.e., exchange) until relatively high nonphysiological temperatures (except for metastable hexagonal Cer 5) is a clear and direct indication of an organized and ordered structure with few hydrophilic channels. This is particularly evident for Cer 2 and Cer 3, which do not undergo exchange of either amide or hydroxyl until very high temperatures. Surprisingly, even the addition of a cis double bond in the acid chain of Cer 3B does not induce exchange at appreciably lower temperatures. The addition of an α-hydroxy group to the ceramide fatty acid chain, as in Cer 5 or Cer 7, permits exchange of both hydroxyl and the amide hydrogen to occur at lower temperatures. Hexagonally packed Cer 5 undergoes complete H → D exchange by 45 °C, indicating that this phase of the α-hydoxylated sphingosine has the least barrier to water penetration of any of the ceramides studied here.

Structural Implications. H → D exchange in Cer 3 and Cer 3B is consistent with the structure published by Dahlen and Pascher on a related Cer 3 molecule, N-tetracosanylphytosphingosine.[22] The structure of this molecule, recreated with

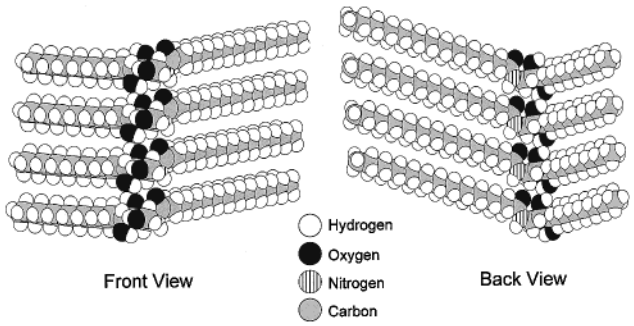

Figure 10. Molecular model of N-tetracosanoylphytosphingosine (C24 Cer 3) from crystallographic data published by Dahlen and Pascher (ref 22).

the original crystallographic data and the addition of hydrogen atoms at standard bond distances, is shown in Figure 10. Anhydrous crystals of this ceramide form a V-shaped structure with tight packing of the amide groups on one side of the V and the three hydroxyl groups tightly packed on the other side of the V. Each of the hydroxyl oxygens participates in two hydrogen bonds, acting both as acceptor and donor. Two hydroxyl groups are H-bonded intramolecularly, while the third hydrogen bonds to an adjacent molecule. This structure allows very little conformational freedom for the headgroup region.

This crystal structure may well be relevant to the hydrated structure. Examination of the vibrational spectra of Cer 3 in the anhydrous state (KBr disk, data not shown) and hydrated shows very similar headgroup behavior. Amide I frequencies are similar to both at 1612 cm^{-1}. The $\nu OH/\nu NH$ frequencies are also very similar. Amide II shows stronger hydrogen bonding (1556 cm^{-1} hydrated, 1545 cm^{-1} crystalline). From this, we infer that the structural organization of the hydroxyls and amides are similar, although not identical, in the crystalline and hydrated states. Because the headgroup modes of the IR spectra of Cer 3 and Cer 3B are also similar, we also infer that Cer 3B has similar headgroup H− bonding to Cer 3.

Unexpectedly, the main effect of hydration is seen in the chains. Anhydrous Cer 3 has orthorhombic chain packing; both δCH_2 and γCH_2 are doublets. In subsequent work,[19] Dahlen and Pascher inferred from X-ray powder diffraction patterns of anhydrous N-tetracosanoylphytospingosine obtained by low temperature cyrstallization that the chains were packed in a more traditional parallel chain bilayer arrangement with orthorhombic symmetry. Hydration of Cer 3 changes chain packing to hexagonal; only single peaks are observed for δCH_2 and γCH_2. The other effect of hydration is to *raise* the temperature of the DSC melting transition for Cer 3 from 110 °C to 115 °C. This effect is opposite to that observed for less well-packed phospholipids such as the phosphatidylcholines, where hydration can lower the transition temperature by more than 50 °C.

Therefore, it appears that the structure of the hydrated ceramides is similar, but not exactly the same, as for their anhydrous crystalline states. Evidently optimal H-bonding of the hydrated phytosphingosine headgroup is incompatible with chain packing in an orthorhombic subcell. However, the headgroup structure observed by Dahlen and Pascher must be similar to the hydrated structure given the similarities in hydroxyl and amide mode frequencies. Strong intermolecular H-bonding is clearly the driving force for Cer 3 and Cer 3B molecular organization, more so when hydrated. This is also consistent with Dahlen and Pascher's observation[19] that at high temperatures, N-tetracosanoylphytosphingosine maintains a high molecular order despite rather mobile chains which he concluded was due to strong intermolecular forces arising from a well-ordered hydrogen bond system.

In Cer 7, addition of an α-hydroxy group to the fatty acid chain allows exchange of the amide and a greater proportion of hydroxyl hydrogens at much lower temperatures than in Cer 3, although chain melting does not occur until 93 °C. This implies that Cer 7 is more open in the headgroup region, but that the hydrogen bonding remains strong and drives molecular organization. Therefore, when hydrated, all phytosphingosines exhibit hexagonal ordered chains and very strong headgroup H-bonding. We conclude that the driving force for molecular self-assembly in the phytosphingosines is headgroup hydrogen bonding.

In contrast to the phytosphingosines, the driving force for molecular self-assembly of the sphingosines appears to be orthorhombic chain packing. Headgroup hydrogen bonding is less strong in the sphingosines, possibly a result of the geometric constraints necessary to achieve orthorhombic chain packing. As long as orthorhombic packing persists, H → D exchange does not occur in the headgroup hydrogens. Once the sphingosine packing changes to hexagonal, the lack of a tight structure driven by strong hydrogen bonding allows some H → D exchange to occur for both hydroxyls and the amide. Therefore, a key aspect of the ability of ceramide bilayers to act as effective barriers to water transport and molecular penetration, at least in pure systems, appears to reside at the 4 position of the base chain. When the 4 position is part of a trans double bond, as in the sphingosines, it allows the molecules to tightly pack into an orthorhombic phase that does not allow molecular penetration. However, when the 4 position contains a hydroxyl group, as in the phytosphingosines, it tightly hydrogen bonds to a hydroxyl group on an adjacent ceramide, also forming a tightly organized structure that does not allow molecular transport.

Implications for Lipid Organization in Stratum Corneum. Although the current work presents molecular structure and organization data for individual ceramides, we believe the results have direct relevance to understanding molecular interactions in the stratum corneum lipid matrix, where ceramides are present with long chain fatty acids and cholesterol. We have previously shown that the sphingosines Cer 2 and Cer 5 form distinct domains in the presence of equimolar amounts of palmitic or stearic acid and cholesterol.[5,16] Therefore, when the driving force for organization of molecular aggregation is the formation of orthorhombic chain packing, the result is the formation of separate domains of sphingosine based ceramides, regardless of molecular environment. However, it is reasonable to assume that with phytosphingosines, whose driving force for organization of molecular aggregation is hydrogen bonding, the presence of other species like fatty acids that can participate in strong hydrogen bonds will result in a very different interaction. In fact, preliminary results in our laboratories indicate that both Cer 3 and Cer 7 strongly interact with fatty acids in the presence of cholesterol to form intimate mixtures that do not phase separate.

These results are also consistent with the fundamental ideas in Forslind's Domain Mosaic model of skin barrier lipid organization.[25,26] Sphingosine ceramides form distinct domains. Phytosphingosine ceramides help join the mosaic domains together through H-bond connections. Acting together, a structure that is relatively water impermeable, yet flexible can result. It will be very interesting to see the role of the 6-hydroxy sphingosine ceramides recently identified by Downing and coworkers.[15]

References and Notes

(1) Schaefer, H.; Redelmeier, T. E. *Skin Barrier: Principles of Percutaneous Absorption*, 1st ed.; Karger: Basel, 1996.
(2) Elias, P. M. *J. Controlled Release* **1991**, *15*, 199−208.
(3) Rawlings, A. V. Skin waxes. Their composition, properties, structures and biological significance. In *Waxes*; Hamilton, R., Christie, W., Eds.; The Oily Press: Dundee, 1995; pp 223−256.
(4) Wertz, P. W.; van den Bergh, B. *Chem. Phys. Lipids* **1998**, *91*, 85−96.
(5) Moore, D. J.; Rerek, M. E.; Mendelsohn, R. *Biochem. Biophys. Res. Commun.* **1997**, *231*, 797−801.
(6) Moore, D. J.; Rerek, M. E.; Mendelsohn, R. *J. Phys. Chem. B* **1997**, *101*, 8933−8940.
(7) Flach, C. R.; Mendelsohn, R.; Rerek, M. E.; Moore, D. J. *J. Phys. Chem. B* **2000**, *104*, 2159−2165.
(8) Mendelsohn, R.; Moore, D. J. In *Methods in Enzymology: Sphingolipid Metabolism and Cell Signaling*; Hannun, Y. A., Merrill, A. H., Eds.; Academic Press: New York, 2000; Vol. 312.
(9) Chen, H.-C.; Mendelsohn, R.; Rerek, M. E.; Moore, D. J. *Biochim. Biophys. Acta* **2000**, *1468*, 293−303.
(10) Hannun, Y. A.; Luberto, C. *Trends in Cell Biology* **2000**, *10*, 73−80.
(11) Merrill, A. H.; Schmelz, E.-M.; Dillehay, D. L.; Spiegel, S.; Shayman, J. A.; Shroeder, J. J.; Riley, R. T.; Voss, K. A.; Wang, E. *Toxicol. Appl. Pharmacol.* **1997**, *142*, 208−255.
(12) Venkataraman, K.; Futerman, A. H. *Trends Cell Biol.* **2000**, *10*, 408−412.
(13) Wertz, P. W.; Miethke, M. C.; Long, S. A.; Strauss, J. S.; Downing, D. T. *J. Invest. Dermatol.* **1985**, *84*, 410−412.
(14) Robson, K. J.; Stewart, M. E.; Michelsen, S.; Lazo, N. D.; Downing, D. T. *J. Lipid Res.* **1994**, *35*, 2060−2068.
(15) Stewart, M. E.; Downing, D. T. *J. Lipid Res.* **1999**, *40*, 1434−1439.
(16) Moore, D. J.; Rerek, M. E. *Acta Derm Venereol* **2000**, *Supp 208*, 16−22.
(17) Mendelsohn, R.; Rerek, M. E.; Moore, D. J. *Phys. Chem. Chem. Phys.* **2000**, *2*, 4651−4657.
(18) Kolter, T.; Sandhoff, K. *Angew. Chem., Int. Ed. Engl.* **1999**, *38*, 1532−1568.
(19) Lofgren, H.; Pascher, I. *Chem. Phys. Lipids* **1977**, *20*, 273−284.
(20) Pascher, I. *Biochim. Biophys. Acta* **1976**, *455*, 433−451.
(21) Karlsson, K.-A. *Acta Biochim. Polonica* **1998**, *45*, 429−438.
(22) Dahlen, B.; Pascher, I. *Acta Crystallogr.* **1972**, *B28*, 2396−2404.
(23) MacPhail, R. A.; Strauss, H. L.; Snyder, R. G.; Ellinger, C. A. *J. Phys. Chem.* **1984**, *88*, 334−341.
(24) Imura, T.; Sakai, H.; Yamauchi, H.; Kozawa, K.; Yokoyama, S.; Matsumoto, M.; Abe, M. *Colliods Surf. B: Biointerfaces* **2000**, *19*, 81−87.
(25) Forslind, B. *Acta Dermato Venereologica* **1994**, *74*, 1−9.
(26) Forslind, B.; Norlen, L.; Engblom, J. *Prog. Colloid Polymer Sci.***1998**, *108*, 10−46.